Failure Criterion For Isotropic Time Dependent Materials Which Accounts for Multi-Axial Loading

D. E. Richardson[2], G. L. Anderson, and D. J. Macon

ATK Thiokol Propulsion Corp., M/S LE1

Brigham City, UT 84302

Abstract

The Space Shuttle's Reusable Solid Rocket Motor (RSRM) nozzle program has recently conducted testing to characterize the effects of multi-axial loading, temperature and time on the failure characteristics of TIGA 321, EA913NA, EA946 (three filled epoxy adhesives). From the test data a "Multi-Axial, Temperature, and Time Dependent" or MATT failure criterion was developed. It is shown that this criterion simplifies, for constant load and constant load rate conditions, into a form that can be easily used for stress analysis. Failure for TIGA 321 and EA913NA are characterized below their glass transition temperature. Failure for EA946 is characterized for conditions that pass through its glass transition. The MATT failure criterion is shown to be accurate for a wide range of conditions for these adhesives.

Kewords: A. Epoxy, B. Steel, C. Stress Analysis, D. Failure Properties

Introduction

Recently, the Space Shuttle's Reusable Solid Rocket Motor (RSRM) nozzle program has conducted testing characterize the effects of multi-axial loading, temperature and time on the failure characteristics of three filled epoxy adhesives (TIGA 321, EA913NA, EA946). As a result of this study, a failure criterion was developed which accounts

---

[2] Corresponding author. Tel.: 435-863-6995; fax: 435-863-2202. E-mail address: david.richardson@atk.com

for these effects. This model was named the "Multi-Axial, Temperature, and Time Dependent" or MATT failure criterion [1,2,3]. Due to the complex nature of the criterion, failure predictions involved use of numerical methods. This paper documents simplifications of the failure criterion for basic loading conditions (constant load and constant load rate) to allow for easier predictions of failure conditions for use with stress analysis evaluations. The paper also documents the verification of the accuracy of this MATT criterion using the three aforementioned adhesives.

Theoretical

The Multi-Axial Temperature and Time (MATT) dependent failure model is as follows [1,2,3].

$$AP^2J_2 + BPI_1 = 1 \tag{1}$$

Here, J_2 is the second deviatoric stress invariant, and I_1 is the first stress invariant. J_2 and I_1 and can be written in the following forms:

$$J_2 = \frac{1}{3}\begin{bmatrix} \sigma_{11}^2 + \sigma_{22}^2 + \sigma_{33}^2 - \\ \sigma_{11}\sigma_{22} - \sigma_{11}\sigma_{33} - \sigma_{22}\sigma_{33} + \\ 3\sigma_{12}^2 + 3\sigma_{13}^2 + 3\sigma_{23}^2 \end{bmatrix} \tag{2}$$

$$I_1 = \sigma_{11} + \sigma_{22} + \sigma_{33} \tag{3}$$

A and B are shape parameters that define shape of the failure envelope (ellipsoidal). These parameters are independent of temperature and time [1,2,3]. This failure criterion is equivalent to the Tsai-Wu [4] and modified Drucker-Prager [5] failure models for a constant P value. P is a factor that defines the size of the failure envelope for a given temperature and failure time. For this paper, the P factor is determined using the following linear cumulative damage model [6]:

$$N_\sigma = \left[\int_0^{t_f} \sigma_i^\beta \, dt\right]^{1/\beta} \tag{4}$$

N_σ and β are failure parameters and σ_i is the applied stress as a function of time. The failure time is t_f. Equation 4 can be simplified for constant load rate (see equation 5) and constant load conditions (see equation 6).

$$t_f = (1+\beta)\left[\frac{N_\sigma}{\sigma_f}\right]^{\beta} \qquad \sigma_f = N_\sigma\left[\frac{t_f}{1+\beta}\right]^{\frac{-1}{\beta}} \tag{5}$$

$$t_f = \left(\frac{N_\sigma}{\sigma_f}\right)^{\beta} \qquad \sigma_f = N_\sigma t_f^{\frac{-1}{\beta}} \tag{6}$$

Incorporating these relationships and normalizing A and B, equation 1 becomes for constant loading rate evaluations:

$$A_\sigma B_\sigma{}^2\left(\frac{t_f}{1+\beta}\right)^{\frac{2}{\beta}} J_2 + B_\sigma\left(\frac{t_f}{1+\beta}\right)^{\frac{1}{\beta}} I_1 = 1 \tag{7}$$

For constant load studies equation 1 becomes:

$$A_\sigma B_\sigma{}^2 t_f^{\frac{2}{\beta}} J_2 + B_\sigma t_f^{\frac{1}{\beta}} I_1 = 1 \tag{8}$$

In this equation, B_σ is a combined MATT failure parameter that contributes to definition of both shape and size of the failure ellipse. B_σ is independent of loading condition (constant load or constant load rate). A_σ defines the shape of the failure envelope ellipsoid and is normalized to the linear cumulative damage term (B_σ...). B has been absorbed into the B_σ term.

It was determined that the B_σ and the β parameters can be approximated as linear functions of temperature for TIGA 321, EA913NA, and EA946 as follows (see Figures 1-6):

$$\beta = m_\beta T + b_\beta \quad (9)$$

$$B_\sigma = m_B T + b_B \quad (10)$$

Here, m_β, b_β, m_B, and b_B are the slope and intercept parameters used to define a line and T is the temperature. The A_σ parameter was found to be nearly constant with temperature and loading rate (see Figures 7-12 and [1-3]).

For these basic loading conditions, substituting equations 9 and 10 into equations 7 and 8 allows for simple failure predictions. As will be demonstrated, these equations can be used to accurately predict failure for a wide range of multi-axial, temperature, and time conditions.

Test Specimens

All testing was conducted using tensile adhesion buttons and napkin ring specimens. All of the adherends were manufactured of either steel or aluminum. Prior to bonding, the adherend surfaces were prepared by washing, grit blasting, and priming (silane based).

The TIGA 321, EA913NA, and EA946 adhesives used are commercially available aromatic and aliphatic amine-cured epoxies. Fiber and/or powder fillers were used in the formulation. The adhesives were vacuum-mixed. RSRM nozzle cure cycles were used for the adhesives.

TIGA 321 and EA913NA are similar adhesives, their stiffnesses are nearly equivalent, but there are differences in their strengths. EA946 is a softer adhesive and has a lower stiffness and strength. This is due to the low glass transition temperature of the adhesive (approximately room temperature). The glass transition temperature of the TIGA 321 and EA913NA is above 50 °C. Testing was conducted at conditions below the glass transition temperature for TIGA 321 and EA913NA. For EA946 testing was conducted at conditions in the glass transition regime. The results of the failure characterization of EA946 are of particular interest due to this low glass-transition temperature.

Within the glass-transition regime the material properties change dramatically with small changes in failure time or temperature. As will be seen, even in this regime of extreme variability the MATT criterion accurately models failure.

Experimental

Significant test data were used to characterize TIGA 321 and EA946 failure. Limited test data were available to characterize failure of EA913NA. Even with the limited amount of characterization data for EA913NA, an accurate failure model was developed.

The time and temperature dependent characteristics of TIGA 321, EA913NA, and EA946 were characterized using tensile adhesion test specimens. These tests allowed for the determination of the m_β, b_β, m_B, and b_B terms. The TIGA 321 m_β and b_β values were used for EA913NA because sufficient data were not available to accurately determine these parameters for this adhesive. Shear adhesion tests were used determine the A_σ parameter (to define the multi-axial loading effects on failure). As will be seen in the data these characterization tests were conducted under temperatures ranging from 20 °C to 45 °C, and with failure times that ranging from several minutes to several hours, and with pure tension loading or pure shear loading.

Verification of the failure model accuracy was evaluated using multi-axial loaded napkin ring test specimens (tension or compression combined with shear) and creep loading (constant load) of tensile adhesion buttons. These failure model verification tests were conducted at temperatures ranging from 20 °C to 45 °C, with failure times ranging from several minutes to several months. It is important to note that predictions of these failure times using the MATT equation involve an extrapolation from the characterization data.

Results and Discussion

The results of tensile adhesion tests can be seen in Figures 13-15 and the results of the shear adhesion tests can be seen in Figures 16-18. All of these tests were used for the MATT characterization of the failure of the adhesives.

Figures 13-18 include both the raw test data and the MATT predictions of failure. Each data point is an average of several tests. The number varies from approximately 5 to 15 depending on the condition, the adhesive, and the test. The coefficients of variation for these characterization tests can be seen in Table 1. As can be seen from the figures and the table, the MATT failure model characterizes tensile adhesion and shear adhesion failure very well.

Figures 19-21 show the multi-axial verification test data and figures 22-24 show the creep verification test data. MATT predictions are provided in all of these figures. Each data point represents the average of approximately 2 to 15 data points. Table 2 contains the coefficients of variation for this verification testing. The test data indicate that the MATT criterion does provide a good prediction of failure for these adhesives.

As would be expected, the coefficients of variation for the adhesive EA946 are higher than those of TIGA 321 and EA913NA. This is due to the fact that EA946 was tested through its glass-transition regime. The coefficients of variation for the EA913NA adhesive are very good considering the limited data and assumptions required to generate the MATT model. It should be noted that the coefficients of variation are very good for the creep adhesion verification testing. Creep failure is notorious for having significant variation.

If all of the test data are combined (characterization and verification), the coefficients of variation found in Table 3 are obtained. It is recognized that these coefficients of variation are somewhat biased due to the disparity in test sample numbers (there are more tensile adhesion tests than creep tests). The data however do indicate that the MATT failure model can be very accurate for a wide range of temperatures, failure times, and multi-axial loading.

Conclusions

The MATT failure criterion has been shown to be readily adaptable to simple loading conditions of constant load and constant load rate. With this feature, predictions of multi-axial, temperature, and time dependent failure can be easily predicted. The failure criterion has been shown to be accurate for three adhesives under a wide range of loading and environmental conditions (time and temperature). The failure predictions for the adhesive EA946 are of particular interest because the MATT model has been verified for a material in the glass transition temperature regime. The

MATT predictions are good even with limited test data, as was seen with the EA913NA predictions. Predictions have been shown to be good even for extrapolation to extended failure times. The test data indicate that the model should be applicable for a wide range of isotropic materials, and that the failure properties can be easily characterized with several key tests.

References

1. Richardson DE, McLennan ML, Anderson GL, Macon DJ, Batista-Rodriguez A. Proc. of the 25th Annual Meeting of The Adhesion Society, Inc. Orlando, 2002. p. 68.
2. Richardson DE, McLennan ML, Anderson GL, Macon DJ, Batista-Rodriguez A. J Adhesion. (in press).
3. Richardson DE, Anderson GL, and Macon DJ, Proceedings of the AIAA JPC, Indianapolis, AIAA-2002-4195, 2002.
4. Tsai SW, Wu EM, J Compos Mater. 1971; 5, p. 58.
5. Drucker DC, Prager W, Q Appl Math. 1952; 10, p. 157.
6. Laheru KL, J. Propuls. Power. 1992; 8, 4, p. 756.

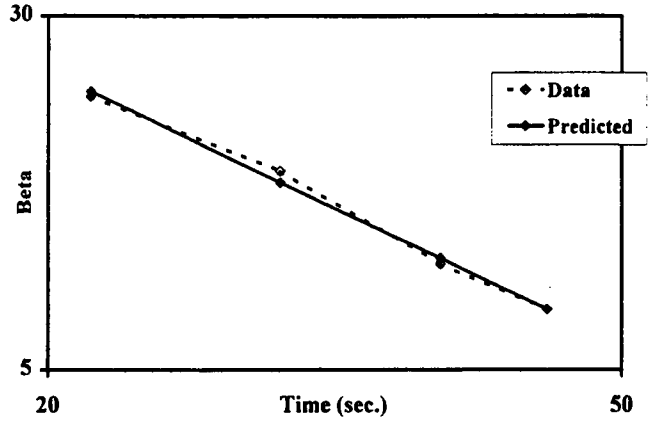

Figure 1. TIGA 321 β Data /Predictions

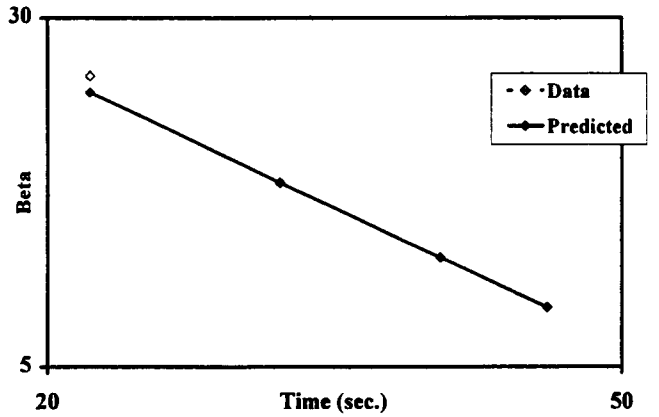

Figure 2. EA913NA β Data /Predictions

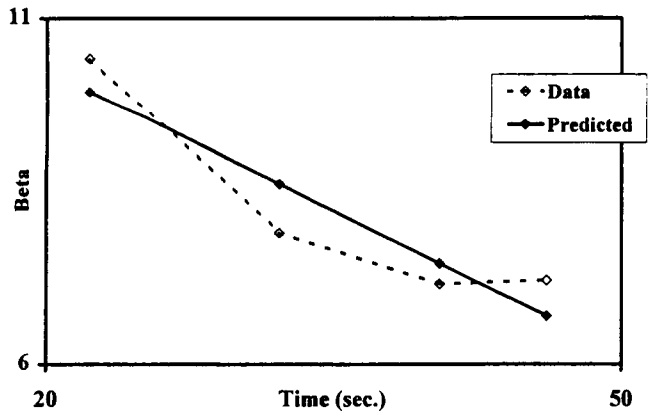

Figure 3. EA946 β Data /Predictions

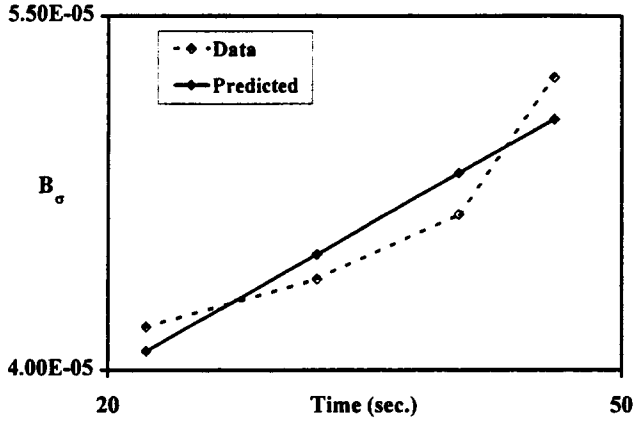

Figure 4. TIGA 321 B_σ Data /Predictions

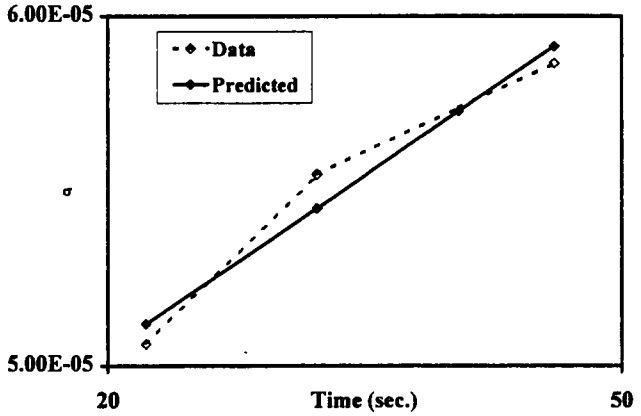

Figure 5. EA913NA B_σ Data /Predictions

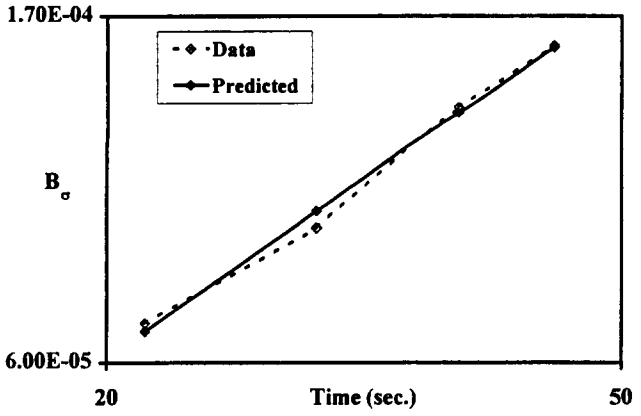

Figure 6. EA946 B_σ Data /Predictions

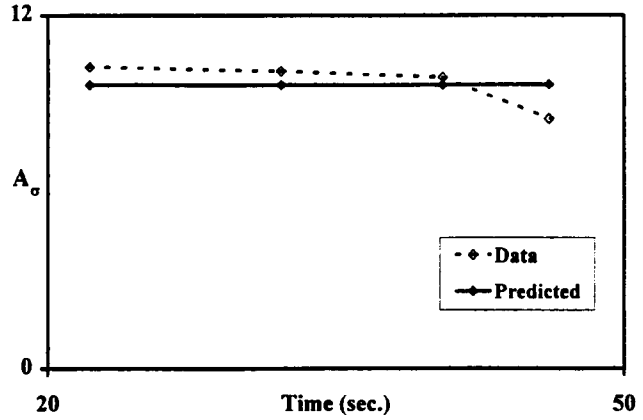

Figure 7. TIGA 321 A_σ Data /Predictions

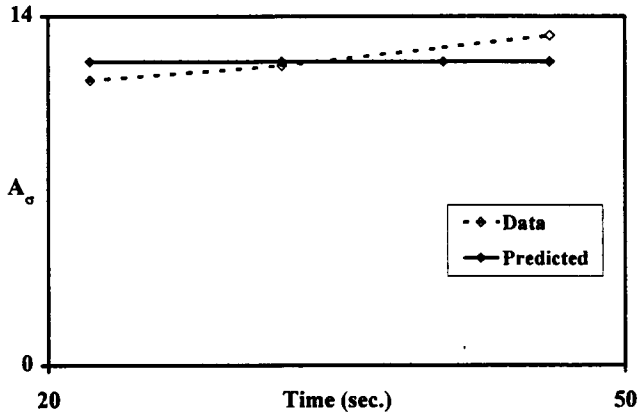

Figure 8. EA913NA A_σ Data /Predictions

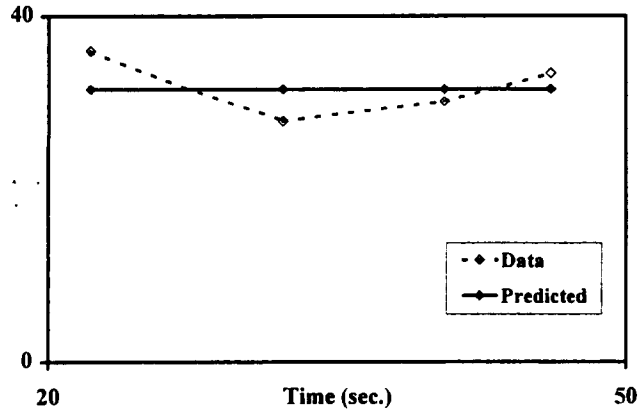

Figure 9. EA946 A_σ Data /Predictions

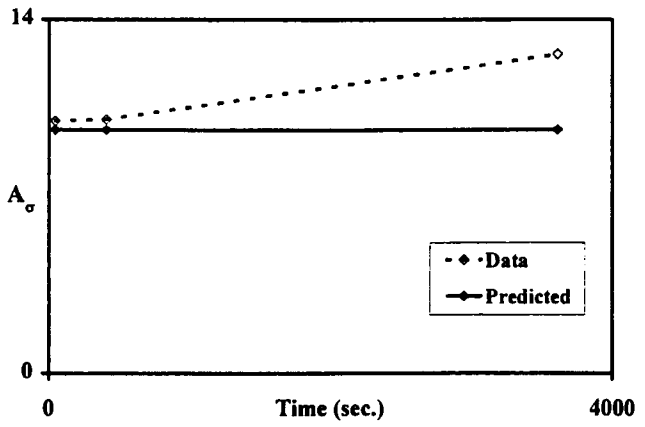

Figure 10. TIGA 321 A_σ Data /Predictions at 20 °F

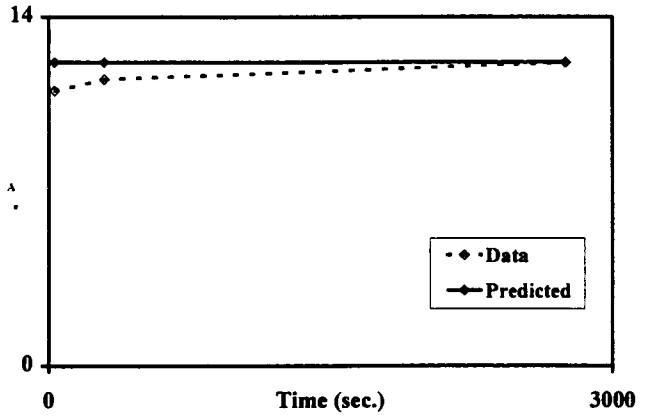

Figure 11. EA913NA A_σ Data /Predictions at 20 °F

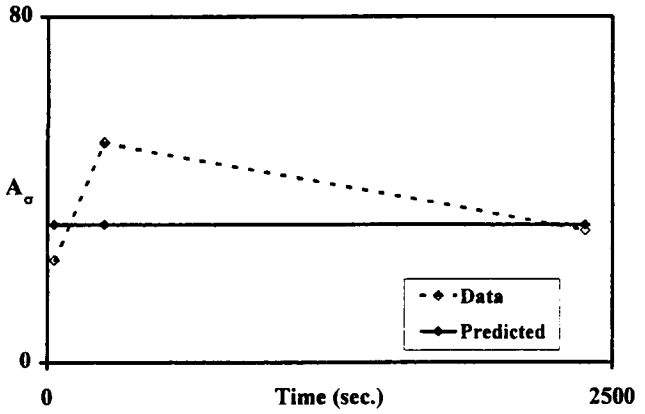

Figure 12. EA946 A_σ Data /Predictions at 20 °F

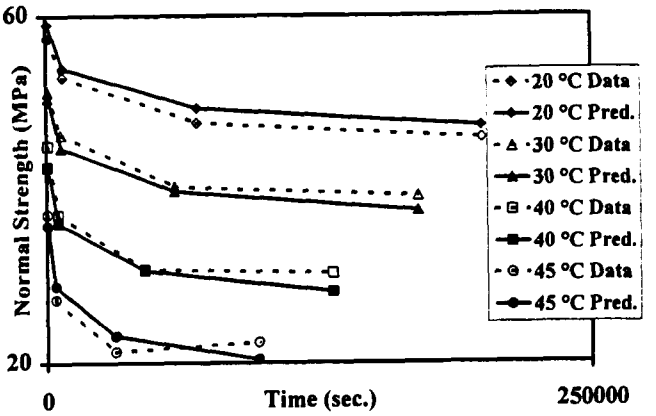

Figure 13. TIGA 321 Tensile Adhesion Data /Predictions

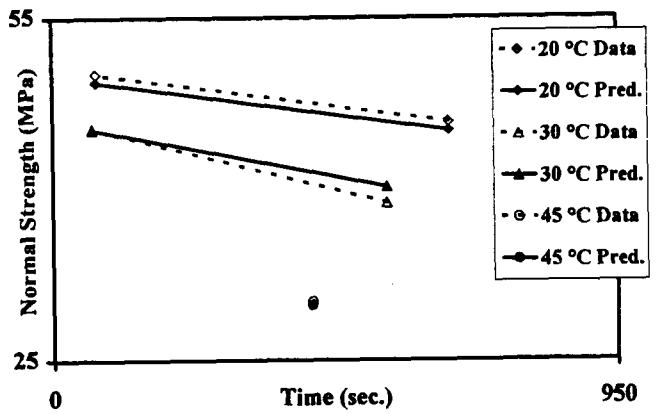

Figure 14. EA913NA Tensile Adhesion Data /Predictions

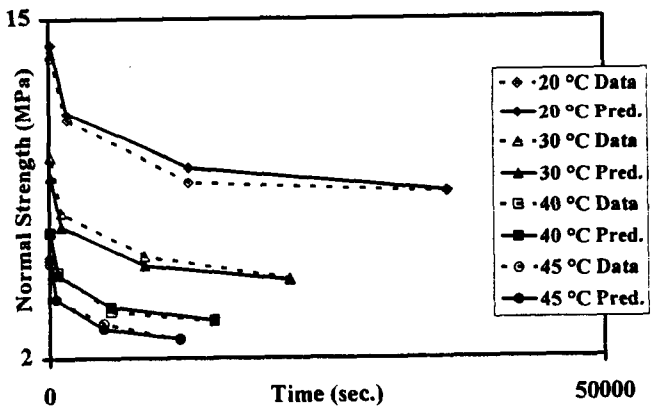

Figure 15. EA946 Tensile Adhesion Data /Predictions

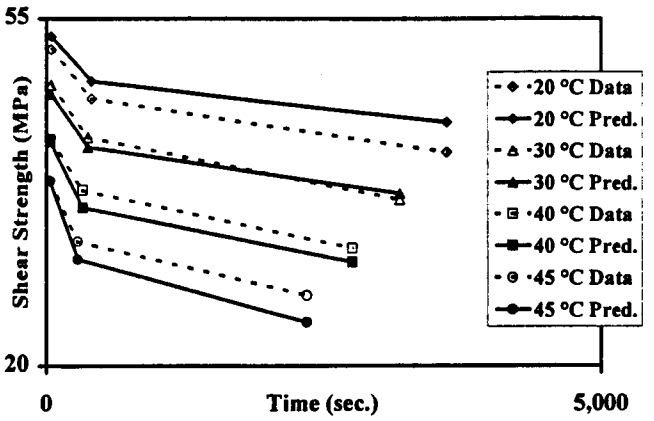

Figure 16. TIGA 321 Shear Adhesion Data /Predictions

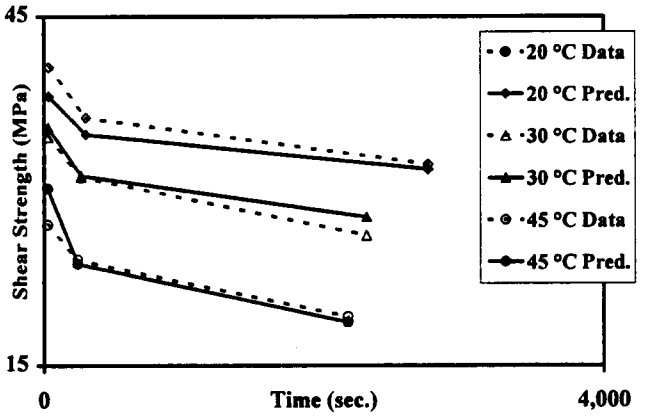

Figure 17. EA913NA Shear Adhesion Data /Predictions

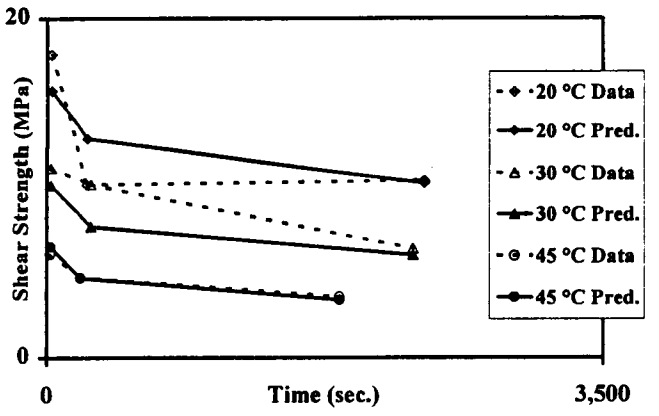

Figure 18. EA946 Shear Adhesion Data /Predictions

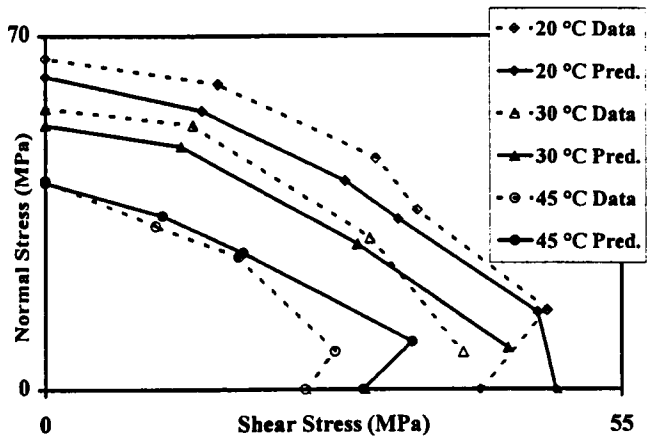

Figure 19. TIGA 321 Multi-Axial Data /Predictions

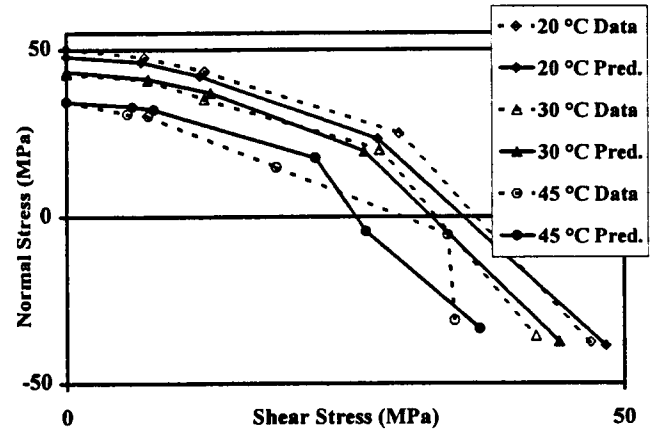

Figure 20. EA913NA Multi-Axial Data /Predictions

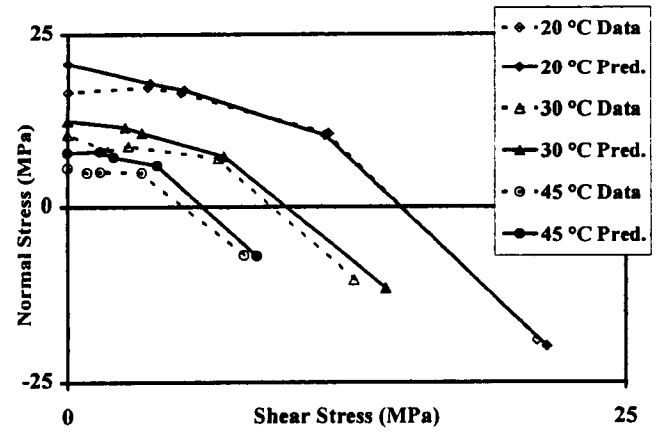

Figure 21. EA946 Multi-Axial Data /Predictions

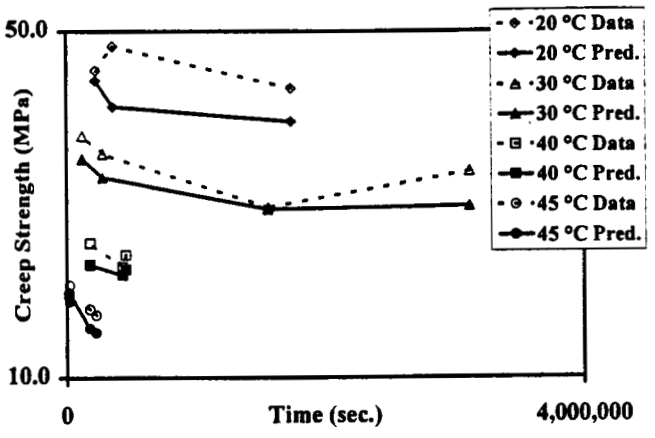

Figure 22. TIGA 321 Creep Data /Predictions

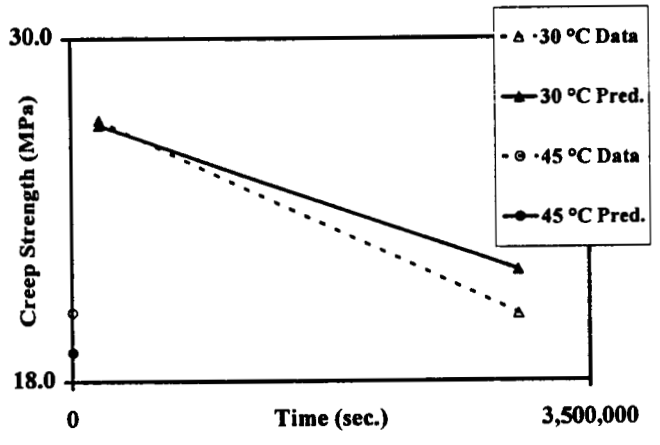

Figure 23. EA913NA Creep Data /Predictions

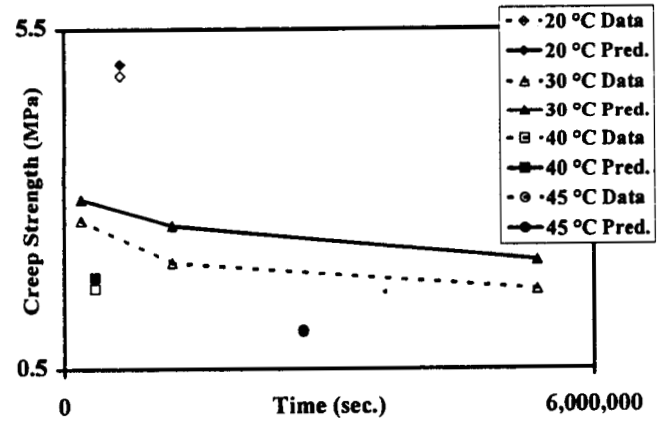

Figure 24. EA946 Creep Data /Predictions

Table 1. Coefficients of Variation for the Tensile Adhesion and Shear Adhesion Tests

Adhesive	Tensile	Shear
TIGA 321	9%	11%
EA913NA	7%	7%
EA946	10%	22%

Table 2. Coefficients of Variation for the Multi-Axial and Creep Tests

Adhesive	Multi-Axial	Creep
TIGA 321	13%	15%
EA913NA	11%	21%
EA946	23%	20%

Table 3. Coefficients of Variation for All Tests

TIGA 321	EA913NA	EA946
11%	9%	17%